

HYBRID STAR MODELS IN THE LIGHT OF NEW MULTI-MESSENGER DATA

JIA JIE LI¹, ARMEN SEDRAKIAN^{2,3}, MARK ALFORD⁴

¹School of Physical Science and Technology, Southwest University, Chongqing 400715, China; jiajieli@swu.edu.cn

²Frankfurt Institute for Advanced Studies, D-60438 Frankfurt am Main, Germany; sedrakian@fias.uni-frankfurt.de

³Institute of Theoretical Physics, University of Wrocław, 50-204 Wrocław, Poland

⁴Department of Physics, Washington University, St. Louis, MO 63130, USA; alford@physics.wustl.edu

Draft version May 21, 2024

ABSTRACT

Recent astrophysical mass inferences of compact stars HESS J1731-347 and PSR J0952-0607, with extremely small and large masses respectively, as well as the measurement of the neutron skin of Ca in the CREX experiment challenge and constrain the models of dense matter. We examine the concept of hybrid stars - objects containing quark cores surrounded by nucleonic envelopes - as models that account for these new data along with other inferences. We employ a family of 81 nucleonic equations of state (EoSs) with variable skewness and slope of symmetry energy at saturation density and a constant speed-of-sound EoS for quark matter. For each nucleonic EoS, a family of hybrid EoSs is generated by varying the transition density, the energy jump, and the speed of sound. These models are tested against the data from GW170817 and J1731-347, which favor low-density soft EoS and J0592-0607 and J0740+6620, which require high-density stiff EoS. The addition of J0592-0607's mass measurement to the constraints has no significant impact on the parameter space of the admissible EoS, but allows us to explore the potential effect of pulsars more massive than J0740+6620, if such exists. We then examine the occurrence of twin configurations and quantify the ranges of masses and radii that they can possess. It is shown that including J1731-347 data favors EoSs that predict low-mass twins with $M \lesssim 1.3 M_{\odot}$ that can be realized if the deconfinement transition density is low. If combined with large speed of sound in quark matter such models allow for maximum masses of hybrid stars in 2.0–2.6 M_{\odot} .

Keywords: Compact objects (228); Neutron stars (1108); Nuclear astrophysics (1129); High energy astrophysics (739)

1. INTRODUCTION

Although the concepts of quark stars and hybrid stars containing a quark core enclosed in a nucleonic envelope were proposed long ago and have been intensively studied over the following decades (for reviews, see [Alford et al. \(2008\)](#); [Anglani et al. \(2014\)](#); [Baym et al. \(2018\)](#); [Sedrakian \(2023\)](#)), they remain at the forefront of the exploration of superdense matter and compact stars (CSs). They may arise through the onset of a first-order phase transition between the nucleonic and quark phases, in which case a new branch of stellar equilibria populated by stable hybrid stars arise. One intriguing aspect of hybrid stars is the existence of twin configurations, i.e., two stars that possess the same mass but different radii, whereby the larger star consists entirely of nucleonic matter, while the more compact star is a hybrid star ([Glendenning & Kettner 2000](#); [Zdunik & Haensel 2013](#); [Benic et al. 2015](#); [Alford & Sedrakian 2017](#); [Alvarez-Castillo et al. 2019](#); [Blaschke et al. 2020](#); [Christian & Schaffner-Bielich 2022](#); [Li et al. 2023a](#)). The study of hybrid stars and their twin configurations continues to be an active area of research, with ongoing efforts to explore their properties and to investigate potential observational signatures that could distinguish them from hadronic CSs (see [Alford et al. 2005](#); [Bonanno & Sedrakian 2012](#); [Masuda et al. 2013](#); [Klähn et al. 2013](#); [Christian et al. 2019](#); [Malfatti et al. 2020](#); [Li et al. 2020](#); [Tan et al. 2020, 2022](#); [Brodie & Haber 2023](#); [Tsaloukidis et al. 2023](#), and references therein).

In recent years, observations of CSs have reached unprecedented levels of precision, providing valuable constraints on the EoS of stellar matter and its composition. Among these constraints, the most interesting ones are depicted in Figure 1.

These include the following:

- (a) The most massive pulsar PSR J0740+6620 ([Fonseca et al. 2021](#)), which has pushed the maximum mass of CSs to 2.0 M_{\odot} .
- (b) The simultaneous mass and radius measurements for PSR J0030+0451 ([Riley et al. 2019](#); [Miller et al. 2019](#)) and J0740+6620 ([Riley et al. 2021](#); [Miller et al. 2021](#)) extracted from X-ray observations using the NICER instrument.
- (c) The detection of gravitational waves from the binary CS merger event GW170817 ([Abbott et al. 2019](#)), which provides us with an estimate of the tidal deformability of the binary that can further yield constraints on the radii of the individual components. Theoretical modeling of GW170817 led to *upper bound* on the mass of a static CS $M \leq 2.3 M_{\odot}$ ([Rezzolla et al. 2018](#); [Shibata et al. 2019](#); [Khadkikar et al. 2021](#)), but it is still uncertain and will not be considered below.
- (d) In addition to these well-established constraints, some new results which are awaiting confirmation, have been reported very recently:
 - (d) The companion of the “black widow” pulsar PSR J0952-0607 (the second-fastest known spinning CS with a frequency of 707 Hz) has been detected in the Milky Way, with a mass estimate of $M = 2.35^{+0.17}_{-0.17} M_{\odot}$ (68% credible interval) ([Romani et al. 2022](#)).
 - (e) The X-ray spectrum of the central compact object within the supernova remnant HESS J1731-347 was modeled and in combination with the distance estimates from Gaia observations yielded a very low mass of $M = 0.77^{+0.20}_{-0.17} M_{\odot}$ and a relatively small radius of $R = 10.4^{+0.86}_{-0.78}$ km (68% credible interval) ([Doroshenko et al. 2022](#)). This modeling substantially revised the previous inference of [Klochkov et al. \(2015\)](#)

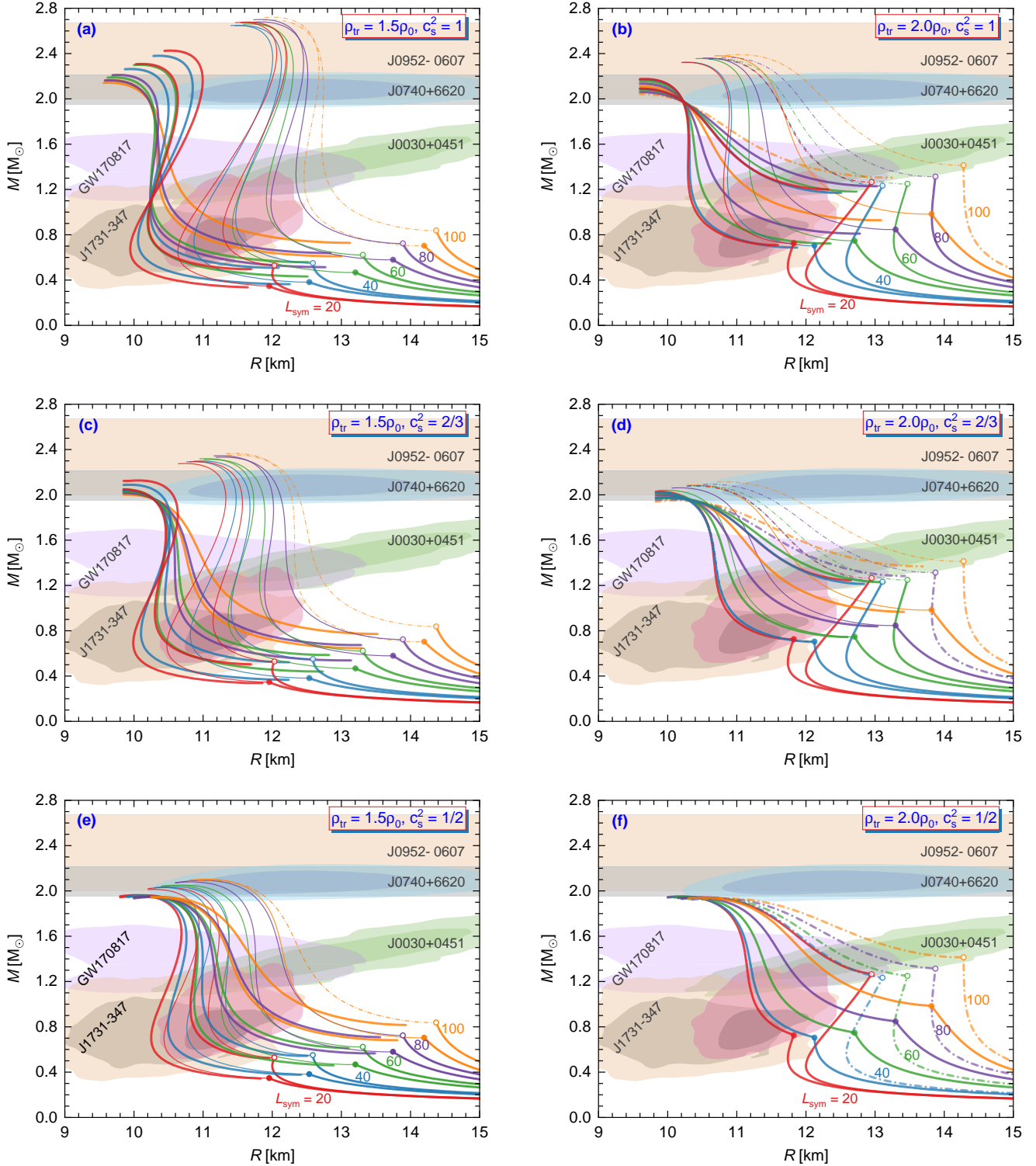


Figure 1. Mass-radius relations for hybrid EoSs with $\rho_{\text{tr}} = 1.5\rho_0$ and $2.0\rho_0$, for $c_s^2 = 1, 2/3$ and $1/2$ in the quark phase. In each panel, the hybrid EoSs are built upon nucleonic models grouped by $L_{\text{sym}} = 20, 40, 60, 80$ and 100 MeV; for each, Q_{sat} is set to -600 and 1000 MeV. The circle on each curve denotes the configuration with central density ρ_{tr} ; lines ending with a filled circle are for the isoscalar-soft nucleonic model with $Q_{\text{sat}} = -600$ MeV and lines ending with an empty circle are for the isoscalar-stiff one with $Q_{\text{sat}} = 1000$ MeV. Observational constraints from multi-messenger astronomy are shown for comparison. The two overlapping regions for HESS J1731-347 (Doroshenko et al. 2022) coincide with areas bounded by solid and dashed lines in their Figure 1. For each nucleonic EoS, the thick line shows the model with a maximum energy jump $\Delta\varepsilon$ that yields hybrid branch passing through the 95% lower limit for the mass-radius constraint of PSR J0740+6620 or J0030+0451, while the thin line shows the model with a critical value of $\Delta\varepsilon$ beyond which a disconnected mass-radius curve arises. Solid lines represent models that are satisfying all constraints, while dash-dotted lines show those failing for J1731-347. Twin configurations arise for reasonable ranges of model parameters and for $c_s^2 = 1$ and $2/3$.

which was based on an alternate value of the distance 3.2 kpc to this object. Doroshenko et al. (2022) show six different ellipses which correspond to a step-wise increase in the realism and improvement of their modeling via: (a) inclusion of data below 1 keV, (b) replacement of the *wabs* simple absorption model developed by Morrison & McCammon (1983) by the *tbabs* model of Wilms et al. (2000) that provides a more accurate description of the absorption process, (c) accounting for the scattering component, (d) fixing the distance to the smaller and more realistic value of 2.5 kpc, and finally (e) using distance priors from the Gaia estimate of the optical companion of HESS J1731-347. As seen from Extended Data Figure 1 in Doroshenko et al. (2022) the steps (d) and (e) shift the mass-radius ellipse to smaller values than previously estimated. The last two ellipses are then considered as the most realistic because they include the most sophisticated physical modeling and the most accurate information on the distance to the object. These authors also provide in their Table 1 best fits using five different atmosphere models. The three models of single-temperature atmospheres provide quantitatively similar values, which are adopted as the most reliable case. The other two-temperature models were considered having fixed $1.4 M_{\odot}$ mass and 12 km radius. The temperatures of the two bright spots and the rest surface as well as the size of the spots were fitting parameters. While it was shown that neutron stars with non-uniform surfaces and the above-quoted conventional mass and radius values can also describe the observed spectra, the absence of pulsation (expected in this case) poses a serious problem for such two-temperature models (V. Suleimanov, private communication).

Given these new inferences, it is worthwhile to take a fresh look at the concept of a hybrid star by allowing for a broad range of admissible parameter space within models that have been tested on a more limited set of observations. In the present work, we implement such a program for the construction of hybrid EoSs and apply filtering to extract the range of EoS that is consistent with the current data. Our further focus is on twin stars and their compatibility with the aforementioned multi-messenger information after the inclusion of extreme domains of masses in our analysis.

2. HYBRID MODELS

To describe low-density matter, we use a covariant density functional of nuclear matter in which baryons are coupled to mesons with density-dependent couplings (Typel & Wolter 1999; Oertel et al. 2017; Sedrakian et al. 2023). The nuclear matter properties are conveniently assessed using the coefficients of Taylor expansion of energy density with respect to the baryon density and isospin asymmetry at the saturation density ρ_0 . The low-order coefficients, the saturation energy E_{sat} , compressibility K_{sat} , and symmetry energy J_{sym} are either strongly constrained or have no noticeable impact on the gross properties (e.g., mass, radius, deformability, etc.) of CSs (Margueron et al. 2018; Li & Sedrakian 2019).

Here we adopt a family of nucleonic EoSs consisting of 81 EoSs that share the same low-order coefficients as the original DDME2 parameterization (Lalazissis et al. 2005), but have alternative density-dependence of the couplings, thus, resulting in different high-order coefficients (Li & Sedrakian 2023). These coefficients and their variations explored in this work are summarized in Table 1. It is worthwhile mentioning that in the calibration of model parameters, we fixed the symmetry energy at the crossing density 0.110 fm^{-3} (which is tightly constrained from finite nuclei properties) as that of DDME2,

Table 1
Nuclear matter characteristics at saturation density.

ρ_0 (fm^{-3})	M_D^* (m_N)	E_{sat} (MeV)	K_{sat} (MeV)	Q_{sat} (MeV)	J_{sym} (MeV)	L_{sym} (MeV)
0.152	0.57	-16.14	251.15	-600 - 1000	28.73 - 36.48	20 - 100

Note. — M_D^* denotes the Dirac effective mass in units of nucleon mass. The symmetry energy at the cross density 0.110 fm^{-3} is fixed as 27.09 MeV the DDME2 value (Li & Sedrakian 2023).

the symmetry energy and its slope coefficient at saturation density are thus correlated (Li & Sedrakian 2023). Specifically, the skewness coefficient for symmetric matter (characterizing the isoscalar sector) varies in the range $-600 \leq Q_{\text{sat}} \leq 1000 \text{ MeV}$ and the slope parameter of the symmetry energy (characterizing the isovector sector) varies in the range $20 \leq L_{\text{sym}} \leq 100 \text{ MeV}$. Note that values of Q_{sat} and L_{sym} control, respectively, the high- and intermediate-density behaviors of the nucleonic EoS, thereby influencing the maximum mass of static nucleonic stars and the radius of the canonical-mass star (Margueron et al. 2018; Li & Sedrakian 2019). The value of L_{sym} , commonly considered to be close to 60 MeV, has been challenged by the recent analyzes of the neutral weak form factor of ^{48}Ca in the CREX experiment, which suggests a rather low value of $L_{\text{sym}} = 20 \pm 30 \text{ MeV}$ (Adhikari et al. 2022). This can be contrasted to the values of $L_{\text{sym}} = 106 \pm 37 \text{ MeV}$ obtained by some groups via the analysis of the neutron skin thickness of ^{208}Pb in the PREX-II experiment (Adhikari et al. 2021). Combined analysis of PREX and CERX experiments favors $L_{\text{sym}} \simeq 60 \text{ MeV}$ (Lattimer 2023). Somewhat larger value $L_{\text{sym}} = 79 \pm 39 \text{ MeV}$ was deduced from collider-based high-energy data involving the determination of the neutron skin of ^{208}Pb at LHC (Giacalone et al. 2023). The ab initio computations predict $L_{\text{sym}} = 37\text{--}66 \text{ MeV}$ (Hu et al. 2022). The lower range $L_{\text{sym}} = 20 \text{ MeV}$ used in our modeling is consistent with the value at which the CREX and PREX ranges begin to overlap as L_{sym} is increased, see Figure 7 of Lattimer (2023).

The quark phase is described by the constant sound speed (CSS) parameterization (Zdunik & Haensel 2013; Alford et al. 2013),

$$p(\varepsilon) = \begin{cases} p_{\text{tr}}, & \varepsilon_{\text{tr}} < \varepsilon < \varepsilon_{\text{tr}} + \Delta\varepsilon, \\ p_{\text{tr}} + c_s^2 [\varepsilon - (\varepsilon_{\text{tr}} + \Delta\varepsilon)], & \varepsilon_{\text{tr}} + \Delta\varepsilon < \varepsilon, \end{cases} \quad (1)$$

where p_{tr} is the pressure and ε_{tr} is the energy density at the phase transition from nucleonic to quark matter at zero temperature and nucleonic density ρ_{tr} ; $\Delta\varepsilon$ is the energy discontinuity and c_s is the sound speed in the quark phase. The first-order phase transition described by this EoS leads to a new stable branch populated by hybrid stars that may or may not be separated from the nucleonic branch by an instability region. Furthermore, for a range of parameters, this leads to the phenomenon of twin configurations — two stable CSs that have identical masses but different radii and consequently, tidal deformabilities (Alford et al. 2013; Benic et al. 2015; Paschalidis et al. 2018; Alvarez-Castillo et al. 2019; Christian et al. 2019; Montana et al. 2019; Christian & Schaffner-Bielich 2021). In this work, we adopt three values of c_s^2 : the maximally stiff EoS with $c_s^2 = 1$ (in natural units) allows us to explore the limits of ranges of masses and radii accessible to models of the type considered in this work; see also Tsouloukidis et al. (2023). The alternative values $c_s^2 = 2/3$ and $1/2$ are intermediate between the maximally stiff and the asymptotic high-density value $c_s^2 = 1/3$ corresponding to a confor-

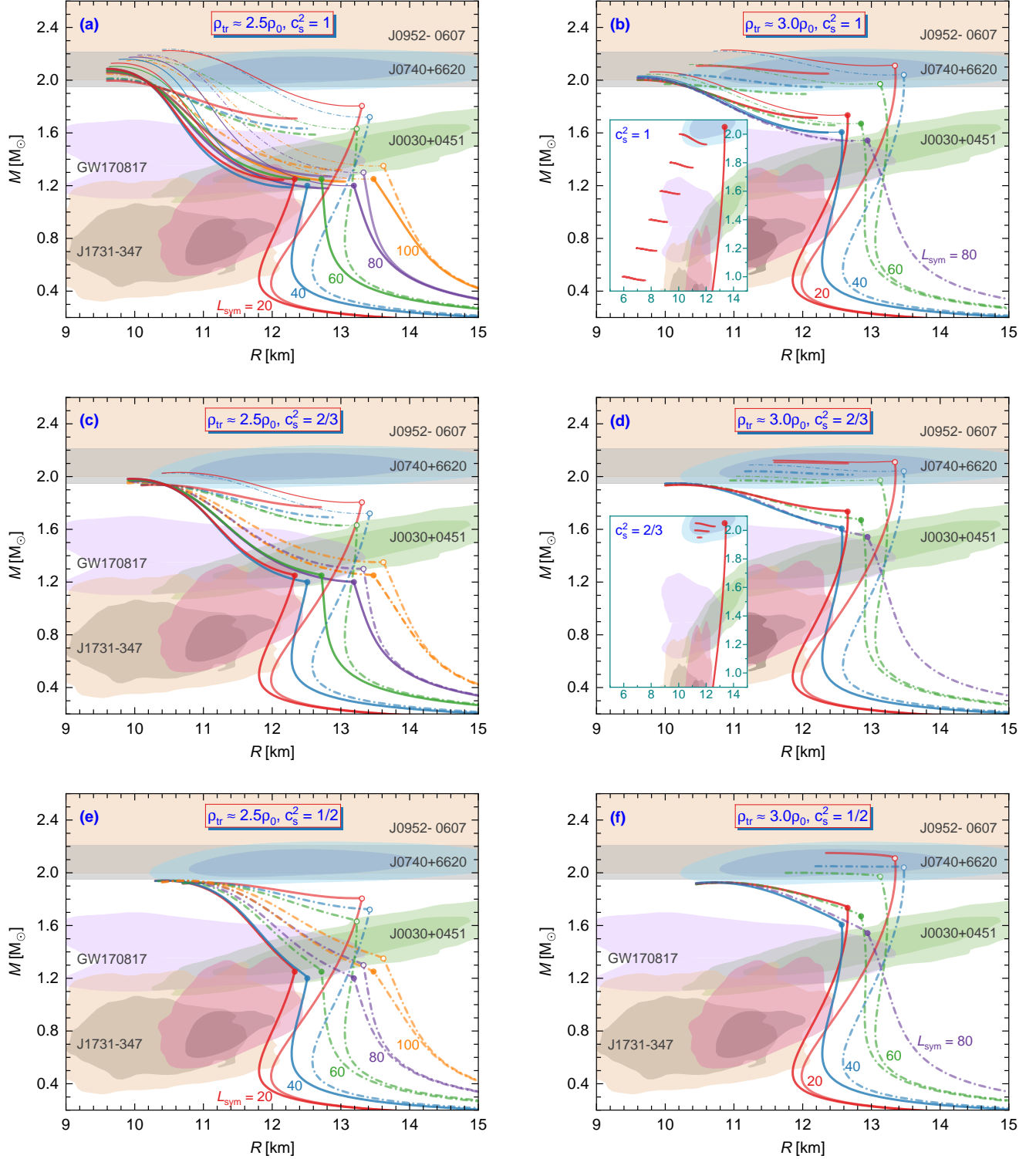


Figure 2. Mass-radius relations for hybrid EoS with $\rho_{\text{tr}} \approx 2.5\rho_0$ and $3.0\rho_0$, for $c_s^2 = 1$, $2/3$ and $1/2$ in the quark phase. In each panel, the hybrid EoS are constructed from nucleonic models grouped by $L_{\text{sym}} = 20, 40, 60, 80$ and 100 MeV; for each, Q_{sat} is chosen such that the resultant mass-radius curve passes through the 95% confidence region for HESS J1731-347 (solid lines) or GW170817 (dash-dotted lines), respectively. The circle on each curve denotes the configurations with central density ρ_{tr} . For each nucleonic EoS, the thick line shows the model with a maximum $\Delta\varepsilon$ that yields a hybrid branch passing through the 95% lower limit for the mass-radius constrain of PSR J0740+6620, while the thin line shows the model with a connected mass-radius curve with a critical value of $\Delta\varepsilon$ set by the constraint for J0740+6620 or appearance of twin configurations. Solid lines represent models satisfying all constraints, while dash-dotted lines show those failing for J1731-347. The inset illustrates hybrid EoS built upon an isoscalar-stiff nucleonic model for the case $M_{\text{max}}^{\text{Q}} \leq M_{\text{max}}^{\text{H}}$ which yields ultra-compact configurations for the case $c_s^2 = 1$.

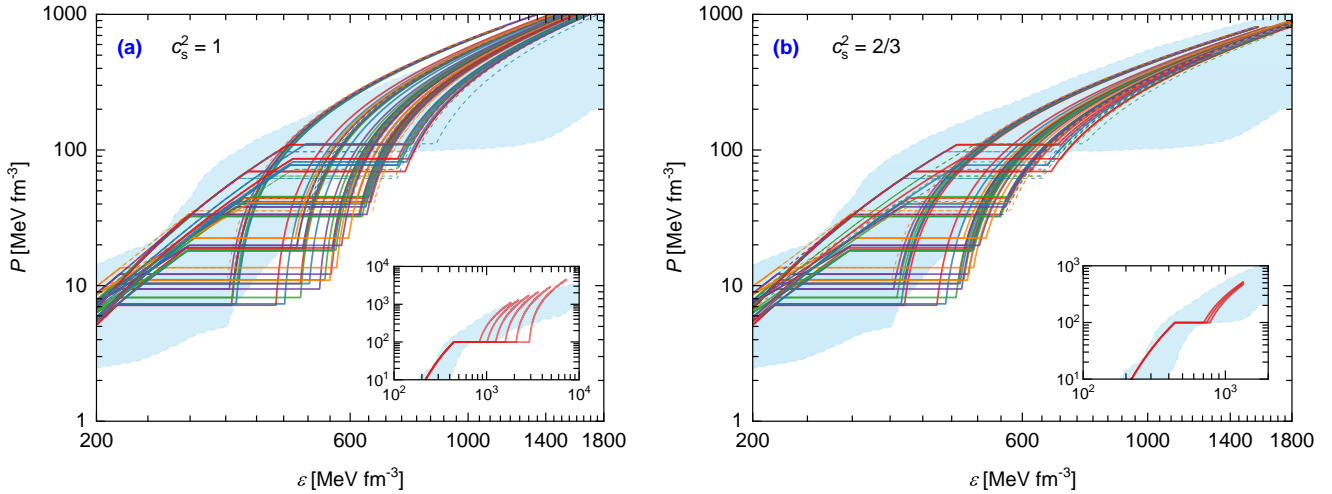


Figure 3. EoS collection utilized in the work. Solid thick lines represent models that satisfy all constraints, while dashed thin lines show those that fail for HESS J1731-347. The blue region shows the allowed range of EoS obtained by imposing $M_{\max} \geq 2.0 M_{\odot}$, $R_{2.0} \geq 11.1$ km and $\tilde{\Lambda}_{\text{GW170817}} \leq 720$ according to [Annala et al. \(2022\)](#) (the yellow area of their Figure 1). This includes EoSs mimicking first-order phase transitions. Insets show EoSs that give rise to ultra-compact stars.

mally symmetric quark phase. Other values of c_s^2 have been considered very recently by several authors ([Brodie & Haber 2023](#); [Sagun et al. 2023](#)) in the context of HESS J1731-347 for alternate nucleonic EoSs.

3. COMPUTATIONAL SCHEME

To cover the parameter space of our model, we choose from the family of 81 nucleonic EoS models given in [Li & Sedrakian \(2023\)](#) a subset which are identified by the values of Q_{sat} and L_{sym} . We then choose the values for $\rho_{\text{tr}} = 1.5, 2.0, 2.5, 3.0\rho_0$ to match these nucleonic EoS to quark matter EoS, for a magnitude of the density jump $\Delta\varepsilon$ and squared sound-of-speed $c_s^2 = 1, 2/3$ or $1/2$.

For each EoS in our collection, we solve the Tolman-Oppenheimer-Volkoff (TOV) equations for static and spherically symmetric stellar objects. If all the mass and radius ranges of astronomical data are intersected by a sequence corresponding to a particular EoS it is accepted, otherwise it is rejected. More specifically, we consider the set of constraints (a)-(c) listed in the Introduction, i.e., those based on NICER inferences of mass and radius for J0030+0451 and J0740+6620, GW170817 inference of radii and masses in the binary CS merger, and radio-wave measurements of the mass of J0740+6620. We then supplement these by the mass and radius of J1731-347 and the mass of J0952-0607. Note that, if we assume uniform rotation, the increase of mass of the maximum-mass configuration due to the rotation of 707 Hz is about of $0.05 M_{\odot}$. Therefore, the lower limit on the mass of J0952-0607 is about the same as that of J0740+6620 at a 95% confidence level. The parameters for quark EoS, ρ_{tr} and $\Delta\varepsilon$, can be transformed into observational properties of CSs, i.e., the maximum mass of the nucleonic branch $M_{\text{max}}^{\text{H}}$ and that of the hybrid branch $M_{\text{max}}^{\text{Q}}$, respectively, in the M - R diagram ([Li et al. 2023b](#)). We further introduce the minimal mass in the hybrid branch, denoted as $M_{\text{min}}^{\text{Q}}$, which we shall use for assessing the range of mass where twin configurations exist.

4. ANALYSIS OF THE RESULTS

Figures 1 and 2 show the M - R diagrams for hybrid EoS models where the nucleonic EoS is specified by values of Q_{sat} and L_{sym} and the quark matter EoS is specified by the sound speed value $c_s^2 = 1, 2/3$ and $1/2$. Figure 1 is for lower transition densities $\rho_{\text{tr}} = 1.5$ or $2.0\rho_0$; Figure 2 is for higher

transition densities $\rho_{\text{tr}} = 2.5$ or $3.0\rho_0$. The isovector properties of nucleonic EoS are measured by the value of L_{sym} . Consider first the isovector-soft (e.g., $L_{\text{sym}} = 20$ MeV) EoSs, which contain members that are consistent with astrophysical constraints at the 95% confidence level for any of the chosen parameters shown in panels of Figures 1 and 2. It is seen that as the transition density increases in the considered range 1.5 - $3.0\rho_0$ the masses of twin stars increase as well. A larger speed of sound allows the hybrid branch to stretch to the region of smaller radii, and more generally to cover a broader range, as can be seen from the ultra-compact members shown in the insets in panels (b, d) of Figure 2. These models can be contrasted with the isovector-stiff (e.g., $L_{\text{sym}} = 80$ MeV) EoSs. In this case, the transition to quark matter needs to occur at a sufficiently low density $\rho_{\text{tr}} \lesssim 2.0\rho_0$, to satisfy the constraints imposed by HESS J1731-347 and GW170817, as displayed in Figure 1. Furthermore, compatibility with the large radius of PSR J0740+6620 is achieved for relatively small energy density discontinuity at the phase transition. The resulting sequences satisfy the two-solar mass constraint because the maximum of the hybrid branch $M_{\text{max}}^{\text{Q}} \sim 2.0 M_{\odot}$, which is also the maximum mass for the entire sequences. In this case, only low-mass twin configurations appear that are consistent with astrophysical constraints. For models with $c_s^2 = 1/2$ twin configurations do not arise in the case of high-density transition from nucleonic to quark matter. They are present only for the lowest transition density $\rho_{\text{tr}} = 1.5\rho_0$.

Figure 3 shows the high-density portion of all the EoSs used in this work, i.e., including those that fail to account for HESS J1731-347. (Models with $c_s^2 = 1/2$ are not shown as they locate well inside the range spanned by $c_s^2 = 2/3$.) The EoSs of ultra-compact stars, with radii in the range $6 \leq R \leq 10$ km and much higher central densities, are separated in the insets. It is seen that the addition of J1731-347 does not change the range of allowed EoS and that the high-density range covered by our collection is broadly compatible with the one deduced in [Annala et al. \(2022\)](#) by imposing current astrophysical constraints on a very large randomly generated ensemble of physics-agnostic EoS covering the intermediate-density range. Some exception is seen among the EoS which feature low transition density ρ_{tr} and large density jump $\Delta\varepsilon$. We also note that the low-density range of the EoS, which can be found in [Li & Sedrakian \(2023\)](#), is consistent with the low-

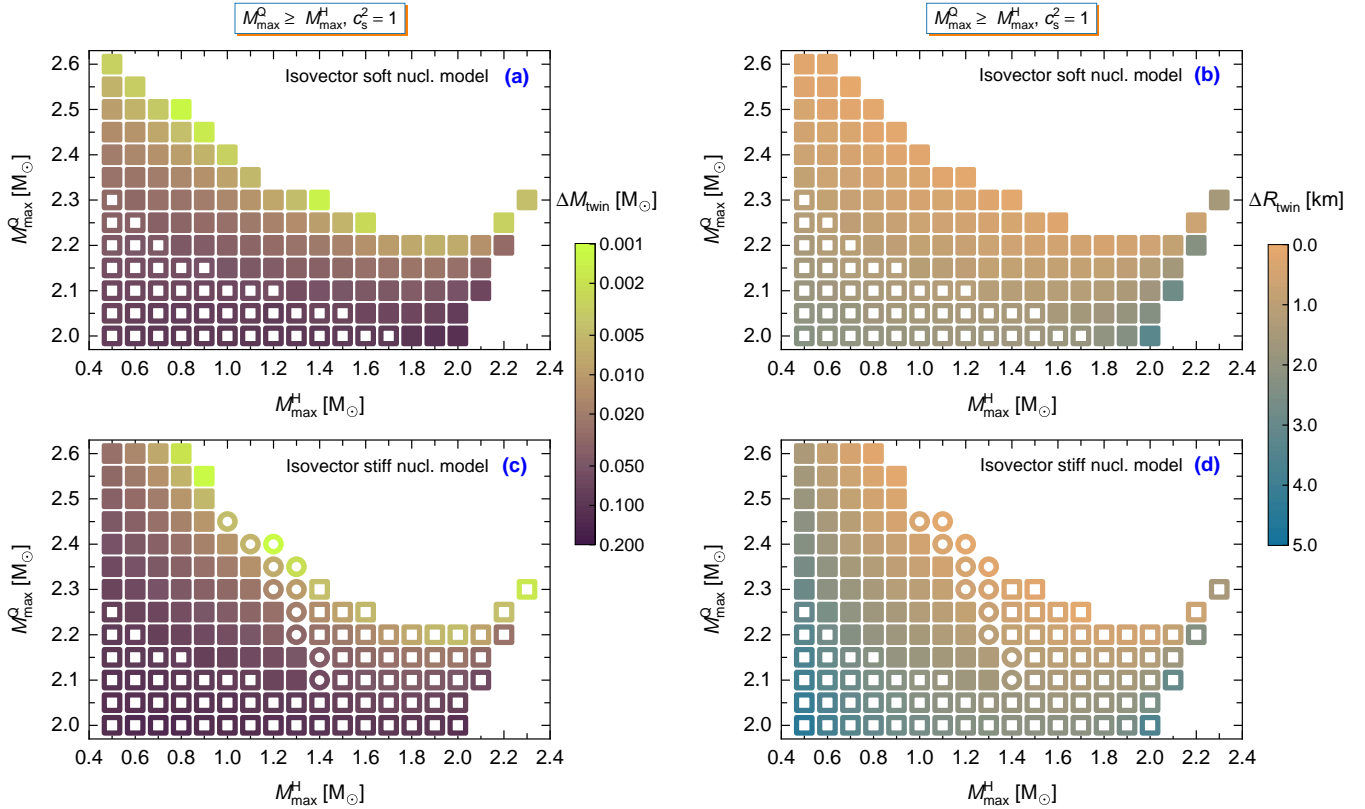


Figure 4. Ranges of mass and radius that characterize twin configurations for the case A, i.e., $M_{\max}^Q \geq M_{\max}^H$. In panels (a, b) the hybrid EoS models ($c_s^2 = 1$) are built using an isovector-soft nucleonic model ($Q_{\text{sat}} = 800$, $L_{\text{sym}} = 20$ MeV), while in panels (c, d) - using an isovector-stiff nucleonic model ($Q_{\text{sat}} = 800$, $L_{\text{sym}} = 80$ MeV). Panels (a, c) show the mass ranges of twins ΔM_{twin} using color coding. Panels (b, d) do the same but for the radii of twin configurations ΔR_{twin} . By open squares, we show the models that are ruled out by combined observational constraints, whereas by open circles we show those that are excluded by HESS J1731-347 data.

density microscopic (chiral) EoS, as presented in [Annala et al. \(2022\)](#), only for $40 \leq L_{\text{sym}} \leq 60$ MeV. Interestingly, despite the large variations of parameters of EoS, all models converge at high density to the region deduced by [Annala et al. \(2022\)](#). This finding is contrary to their conclusion that perturbative QCD highly constrains nuclear matter properties at intermediate densities.

To facilitate the following discussion, we divided the stellar configurations into those where the maximum-mass star is on the hybrid branch (case A) and those where the maximum-mass star is on the nucleonic branch (case B). This type of classification has been considered previously; case A was studied in [Li et al. \(2021\)](#) and [Christian & Schaffner-Bielich \(2022\)](#) and case B in [Li et al. \(2023a\)](#).

Case A: Figure 4 summarizes the contours representing the ranges of mass and radius that characterize twin configurations for hybrid EoS models with $M_{\max}^H \leq M_{\max}^Q$ for $c_s^2 = 1$. Filled symbols indicate models that satisfy astrophysical constraints, while empty symbols represent models that do not. The color of the square shows the range of mass or radius over which twins can be found. The cases $c_s^2 = 2/3$ and $1/2$ in Figure 5 show the same trends but the ranges of masses and radii are significantly narrower. The shape of the sequences in Case A dictates that the range of masses where twin configurations exist is defined as $\Delta M_{\text{twin}} = M_{\max}^H - M_{\min}^Q$. Then, the differences in radii ΔR_{twin} for twin configurations is determined by comparing the radius of M_{\max}^H nucleonic star to that of the hybrid counterpart with an identical mass. It can be observed from Figures 1 and 2 that this is also the maximal radius difference for a hybrid EoS predicting twin configura-

tions. A lesson that we learn from Figures 4 and 5 is that the possible combinations M_{\max}^Q and M_{\max}^H for which twin configurations exist is large for the isovector-soft nucleonic model [(panel (a))] and is small for the isovector-stiff model [(panel (c))]. Also these two cases predict different M_{\max}^Q and M_{\max}^H for which the largest range of masses $\leq 0.2 M_{\odot}$ (shown by dark squares) is achieved. The corresponding values of ΔR_{twin} shown in panels (b, d) indicate that the largest difference between the twin radii is achieved for sequences that have both maxima around the two-solar mass. The twin configurations with $\Delta R_{\text{twin}} \sim 4\text{--}5$ km correspond to low-mass hybrid stars relevant for HESS J1731-347.

Case B: Figure 6 summarizes the ranges of masses and radii that characterize twin configurations for hybrid EoS models in the case $M_{\max}^Q \leq M_{\max}^H$, for $c_s^2 = 1$. Here the range of masses is defined $\Delta M_{\text{twin}} = M_{\max}^Q - M_{\min}^H$ and the differences in radii ΔR_{twin} is extracted from the radius of M_{\max}^Q hybrid star and its nucleonic twin. For such cases, as illustrated in the insets of Figure 2, we require the nucleonic branch passing through all the 95% confidence regions of constraints, this can be achieved only for isovector-soft models and the values of c_s^2 close but below unity ([Li et al. 2023a](#)). It is seen that ultra-compact configurations with radii $6 \leq R \leq 10$ km, associated with large values of ΔR_{twin} , are present only for models with $M_{\max}^H \approx 2.0\text{--}2.15 M_{\odot}$. These ultra-compact members studied in more detail in [Li et al. \(2023a\)](#) together with those appearing in case A offer an alternative to strange stars, which up until recently were considered as the only possible objects with small radii (of the order of 6–9 km) (see [Bombaci et al. 2021](#), and references therein). It is worthwhile also to mention

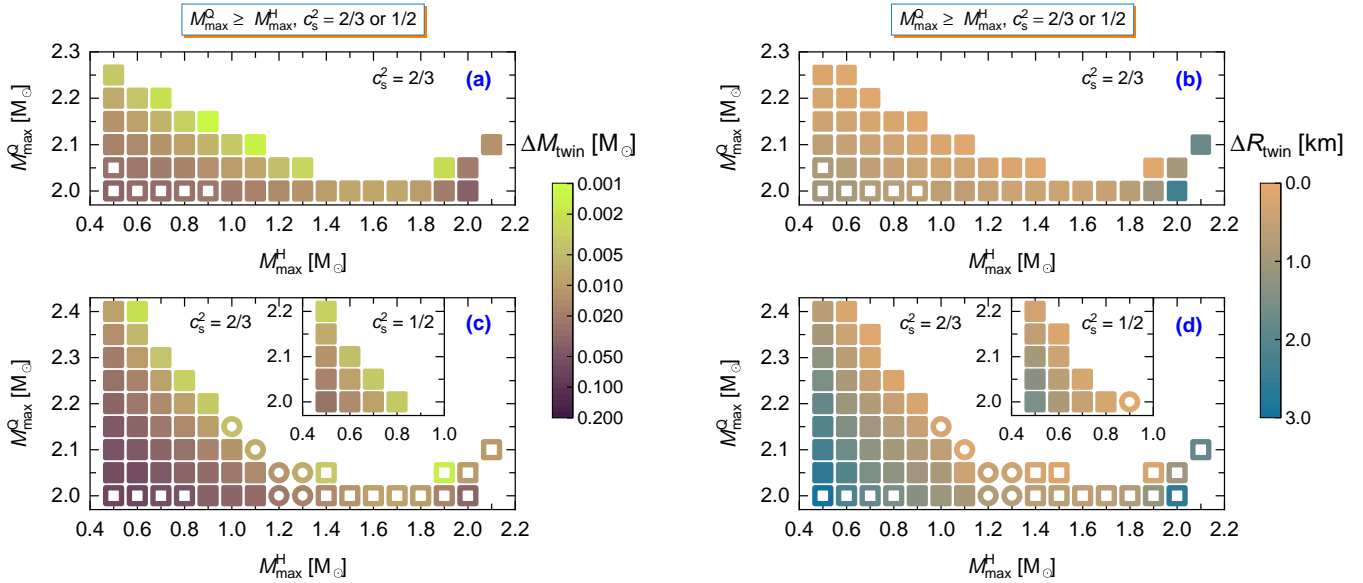


Figure 5. Same as in Figure 4 but for models with intermediate values of $c_s^2 = 2/3$ and $1/2$ (shown as insets). Low-mass twin configurations persist only for the isovector-stiff nucleonic model.

that the maximum-mass values found for hybrid EoSs featuring twin configurations in this case are well within the range of mass obtained for PSR J0592-0607 at a 95% confidence level (Romani et al. 2022).

5. CONCLUSIONS

In this work, we investigated the consistency of the hybrid star models with the current astrophysical and laboratory data and explored the range of parameters that lead to twin stars. To do so, we employed a recently constructed family of nucleonic EoSs parameterized by the Q_{sat} and L_{sym} parameters of the Taylor expansion of the energy density of nucleonic matter. This was then combined with a CSS parameterization of the quark matter EoS for a range of values of the transition density, energy density jump, and sound speed. We

have identified two classes of models with low and high transition densities (as shown in Figures 1 and 2, respectively) that are consistent with the current data. This is achieved through a compromise between the requirement for a soft EoS at low densities, driven by the data from HESS J1731-347 and GW170817, and the need for stiff EoS at high densities to account for the radio-astronomy data for PSR J0592-0607 and J0740+6620. The ranges of parameters of twin configurations that are allowed by our hybrid models were found as shown in Figures 4 and 6. Notably, the data from J1731-347 supports the existence of low-mass twin configurations with masses $M \lesssim 1.3 M_\odot$, regardless of the chosen nucleonic EoS, but it requires a low value for the transition density. These hybrid models also allow for maximum masses M_{max}^Q ranging from 2.0 to 2.6 M_\odot depending on the value of the sound speed in quark matter. In addition, ultra-compact configurations, which lie outside the constraints imposed by GW170817 and J1731-347, emerge for isoscalar-stiff nucleonic EoS models and for large speed-of-sound $c_s^2 = 1$ in the case where the nucleonic branch extends up to 2.0–2.15 M_\odot .

In conclusion, the current astrophysical and nuclear physics data do not rule out hybrid stars, and leave room for hybrid-nucleonic mass twins if a strong first-order phase transition occurs in dense matter for reasonable values of nucleonic isoscalar and isovector characteristics. It is even plausible to argue that all the stars with observational information we have considered in this study are hybrid configurations. But this does not exclude the possibility that current observational data are accounted for by the nucleonic branch of hybrid sequences, whereas the hybrid branch lies outside of ranges currently covered, as would be the case for ultra-compact members of sequences.

ACKNOWLEDGEMENTS

J. L. acknowledges the support of the National Natural Science Foundation of China (Grant No. 12105232), the Fundamental Research Funds for the Central Universities (Grant No. SWU-020021), and by the Venture & Innovation Support Program for Chongqing Overseas Returnees (Grant No. CX2021007). A. S. acknowledges the DFG Grant No. SE 1836/5-2 and the Polish NCN Grant No.

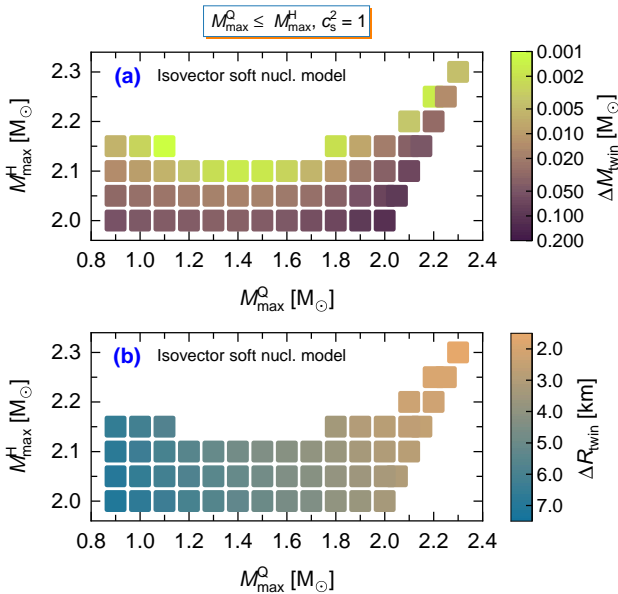


Figure 6. Same as in Figure 4 but for the case B corresponding to $M_{\text{max}}^Q \leq M_{\text{max}}^H$. The hybrid EoS models ($c_s^2 = 1$) are built upon an isovector-soft nucleonic model ($Q_{\text{sat}} = 800$, $L_{\text{sym}} = 20$ MeV). Ultra-compact configurations having large ΔR_{twin} are present only for models with $M_{\text{max}}^H \approx 2.0$ –2.15 M_\odot .

2020/37/B/ST9/01937 at Wrocław University. M. A. is partly supported by the U.S. Department of Energy, Office of Science, Office of Nuclear Physics under Award No. DE-FG02-05ER41375.

REFERENCES

- Abbott, B. P., Abbott, R., Abbot, T. D., et al. 2019, *PhRvX*, 9, 011001, doi: [10.1103/PhysRevX.9.011001](https://doi.org/10.1103/PhysRevX.9.011001)
- Adhikari, D., Albataineh, H., Androic, D., et al. 2021, *PhRvL*, 126, 172502, doi: [10.1103/PhysRevLett.126.172502](https://doi.org/10.1103/PhysRevLett.126.172502)
- . 2022, *PhRvL*, 129, 042501, doi: [10.1103/PhysRevLett.129.042501](https://doi.org/10.1103/PhysRevLett.129.042501)
- Alford, M., Braby, M., Paris, M. W., & Reddy, S. 2005, *ApJ*, 629, 969, doi: [10.1086/430902](https://doi.org/10.1086/430902)
- Alford, M., & Sedrakian, A. 2017, *PhRvL*, 119, 161104, doi: [10.1103/PhysRevLett.119.161104](https://doi.org/10.1103/PhysRevLett.119.161104)
- Alford, M. G., Han, S., & Prakash, M. 2013, *PhRvD*, 88, 083013, doi: [10.1103/PhysRevD.88.083013](https://doi.org/10.1103/PhysRevD.88.083013)
- Alford, M. G., Schmitt, A., Rajagopal, K., & Schäfer, T. 2008, *RvMP*, 80, 1455, doi: [10.1103/RevModPhys.80.1455](https://doi.org/10.1103/RevModPhys.80.1455)
- Alvarez-Castillo, D. E., Blaschke, D. B., Grunfeld, A. G., & Pagura, V. P. 2019, *PhRvD*, 99, 063010, doi: [10.1103/PhysRevD.99.063010](https://doi.org/10.1103/PhysRevD.99.063010)
- Anglani, R., Casalbuoni, R., Ciminale, M., et al. 2014, *RvMP*, 86, 509, doi: [10.1103/RevModPhys.86.509](https://doi.org/10.1103/RevModPhys.86.509)
- Annala, E., Gorda, T., Katerini, E., et al. 2022, *PhRvX*, 12, 011058, doi: [10.1103/PhysRevX.12.011058](https://doi.org/10.1103/PhysRevX.12.011058)
- Baym, G., Hatsuda, T., Kojo, T., et al. 2018, *RPPH*, 81, 056902, doi: [10.1088/1361-6633/aaae14](https://doi.org/10.1088/1361-6633/aaae14)
- Benic, S., Blaschke, D., Alvarez-Castillo, D. E., Fischer, T., & Typel, S. 2015, *A&A*, 577, A40, doi: [10.1051/0004-6361/201425318](https://doi.org/10.1051/0004-6361/201425318)
- Blaschke, D., Ayriyan, A., Alvarez-Castillo, D. E., & Grigorian, H. 2020, *Univ*, 6, 81, doi: [10.3390/universe6060081](https://doi.org/10.3390/universe6060081)
- Bombaci, I., Drago, A., Logoteta, D., Pagliara, G., & Vidana, I. 2021, *PhRvL*, 126, 162702, doi: [10.1103/PhysRevLett.126.162702](https://doi.org/10.1103/PhysRevLett.126.162702)
- Bonanno, L., & Sedrakian, A. 2012, *A&A*, 539, A16, doi: [10.1051/0004-6361/201117832](https://doi.org/10.1051/0004-6361/201117832)
- Brodie, L., & Haber, A. 2023, *PhRvC*, 108, 025806, doi: [10.1103/PhysRevC.108.025806](https://doi.org/10.1103/PhysRevC.108.025806)
- Christian, J.-E., & Schaffner-Bielich, J. 2021, *PhRvD*, 103, 063042, doi: [10.1103/PhysRevD.103.063042](https://doi.org/10.1103/PhysRevD.103.063042)
- Christian, J.-E., & Schaffner-Bielich, J. 2022, *ApJ*, 935, 122, doi: [10.3847/1538-4357/ac75cf](https://doi.org/10.3847/1538-4357/ac75cf)
- Christian, J.-E., Zacchi, A., & Schaffner-Bielich, J. 2019, *PhRvD*, 99, 023009, doi: [10.1103/PhysRevD.99.023009](https://doi.org/10.1103/PhysRevD.99.023009)
- Doroshenko, V., Suleimanov, V., Pühlhofer, G., & Santangelo, A. 2022, *NatAs*, 6, 1444, doi: [10.1038/s41550-022-01800-1](https://doi.org/10.1038/s41550-022-01800-1)
- Fonseca, E., Cromartie, H. T., Pennucci, T. T., et al. 2021, *ApJL*, 915, L12, doi: [10.3847/2041-8213/ac03b8](https://doi.org/10.3847/2041-8213/ac03b8)
- Giacalone, G., Nijs, G., & van der Schee, W. 2023, *PhRvL*, 131, 202302, doi: [10.1103/PhysRevLett.131.202302](https://doi.org/10.1103/PhysRevLett.131.202302)
- Glendenning, N. K., & Kettner, C. 2000, *A&A*, 353, L9, <https://arxiv.org/abs/astro-ph/9807155>
- Hu, B., Jiang, W., Miyagi, T., et al. 2022, *NatPh*, 18, 1196, doi: [10.1038/s41567-022-01715-8](https://doi.org/10.1038/s41567-022-01715-8)
- Khadkikar, S., Raduta, A. R., Oertel, M., & Sedrakian, A. 2021, *PhRvC*, 103, 055811, doi: [10.1103/PhysRevC.103.055811](https://doi.org/10.1103/PhysRevC.103.055811)
- Klähn, T., Łastowiecki, R., & Blaschke, D. B. 2013, *PhRvD*, 88, 085001, doi: [10.1103/PhysRevD.88.085001](https://doi.org/10.1103/PhysRevD.88.085001)
- Klochkov, D., Suleimanov, V., Pühlhofer, G., et al. 2015, *A&A*, 573, A53, doi: [10.1051/0004-6361/201424683](https://doi.org/10.1051/0004-6361/201424683)
- Lalazisis, G. A., Niksic, T., Vretenar, D., & Ring, P. 2005, *PhRvC*, 71, 024312, doi: [10.1103/PhysRevC.71.024312](https://doi.org/10.1103/PhysRevC.71.024312)
- Lattimer, J. M. 2023, *Particles*, 6, 30, doi: [10.3390/particles6010003](https://doi.org/10.3390/particles6010003)
- Li, J. J., & Sedrakian, A. 2019, *ApJL*, 874, L22, doi: [10.3847/2041-8213/ab1090](https://doi.org/10.3847/2041-8213/ab1090)
- . 2023, *ApJ*, 957, 41, doi: [10.3847/1538-4357/acfa73](https://doi.org/10.3847/1538-4357/acfa73)
- Li, J. J., Sedrakian, A., & Alford, M. 2020, *PhRvD*, 101, 063022, doi: [10.1103/PhysRevD.101.063022](https://doi.org/10.1103/PhysRevD.101.063022)
- . 2021, *PhRvD*, 104, L121302, doi: [10.1103/PhysRevD.104.L121302](https://doi.org/10.1103/PhysRevD.104.L121302)
- . 2023a, *PhRvD*, 107, 023018, doi: [10.1103/PhysRevD.107.023018](https://doi.org/10.1103/PhysRevD.107.023018)
- . 2023b, *ApJ*, 944, 206, doi: [10.3847/1538-4357/acb688](https://doi.org/10.3847/1538-4357/acb688)
- Malfatti, G., Orsaria, M. G., Ranea-Sandoval, I. F., Contrera, G. A., & Weber, F. 2020, *PhRvD*, 102, 063008, doi: [10.1103/PhysRevD.102.063008](https://doi.org/10.1103/PhysRevD.102.063008)
- Margueron, J., Hoffmann Casali, R., & Gulminelli, F. 2018, *PhRvC*, 97, 025806, doi: [10.1103/PhysRevC.97.025806](https://doi.org/10.1103/PhysRevC.97.025806)
- Masuda, K., Hatsuda, T., & Takatsuka, T. 2013, *ApJ*, 764, 12, doi: [10.1088/0004-637X/764/1/12](https://doi.org/10.1088/0004-637X/764/1/12)
- Miller, M. C., Lamb, F. K., Dittmann, A. J., et al. 2019, *ApJL*, 887, L24, doi: [10.3847/2041-8213/ab50c5](https://doi.org/10.3847/2041-8213/ab50c5)
- . 2021, *ApJL*, 918, L28, doi: [10.3847/2041-8213/ac089b](https://doi.org/10.3847/2041-8213/ac089b)
- Montana, G., Tolos, L., Hanauske, M., & Rezzolla, L. 2019, *PhRvD*, 99, 103009, doi: [10.1103/PhysRevD.99.103009](https://doi.org/10.1103/PhysRevD.99.103009)
- Morrison, R., & McCammon, D. 1983, *ApJ*, 270, 119, doi: [10.1086/161102](https://doi.org/10.1086/161102)
- Oertel, M., Hempel, M., Klähn, T., & Typel, S. 2017, *RvMP*, 89, 015007, doi: [10.1103/RevModPhys.89.015007](https://doi.org/10.1103/RevModPhys.89.015007)
- Paschalidis, V., Yagi, K., Alvarez-Castillo, D., Blaschke, D. B., & Sedrakian, A. 2018, *PhRvD*, 97, 084038, doi: [10.1103/PhysRevD.97.084038](https://doi.org/10.1103/PhysRevD.97.084038)
- Rezzolla, L., Most, E. R., & Weih, L. R. 2018, *ApJL*, 852, L25, doi: [10.3847/2041-8213/aaa401](https://doi.org/10.3847/2041-8213/aaa401)
- Riley, T. E., Watts, A. L., Bogdanov, S., et al. 2019, *ApJL*, 887, L21, doi: [10.3847/2041-8213/ab481c](https://doi.org/10.3847/2041-8213/ab481c)
- Riley, T. E., Watts, A. L., Ray, P. S., et al. 2021, *ApJL*, 918, L27, doi: [10.3847/2041-8213/ac0a81](https://doi.org/10.3847/2041-8213/ac0a81)
- Romani, R. W., Kandel, D., Filippenko, A. V., Brink, T. G., & Zheng, W. 2022, *ApJL*, 934, L17, doi: [10.3847/2041-8213/ac8007](https://doi.org/10.3847/2041-8213/ac8007)
- Sagun, V., Giangrandi, E., Dietrich, T., et al. 2023, *ApJ*, 958, 49, doi: [10.3847/1538-4357/acfc9e](https://doi.org/10.3847/1538-4357/acfc9e)
- Sedrakian, A. 2023, *Particles*, 6, 713, doi: [10.3390/particles6030044](https://doi.org/10.3390/particles6030044)
- Sedrakian, A., Li, J. J., & Weber, F. 2023, *PrPNP*, 131, 104041, doi: [10.1016/j.pnpnp.2023.104041](https://doi.org/10.1016/j.pnpnp.2023.104041)
- Shibata, M., Zhou, E., Kiuchi, K., & Fujibayashi, S. 2019, *PhRvD*, 100, 023015, doi: [10.1103/PhysRevD.100.023015](https://doi.org/10.1103/PhysRevD.100.023015)
- Tan, H., Dore, T., Dexheimer, V., Noronha-Hostler, J., & Yunes, N. 2022, *PhRvD*, 105, 023018, doi: [10.1103/PhysRevD.105.023018](https://doi.org/10.1103/PhysRevD.105.023018)
- Tan, H., Noronha-Hostler, J., & Yunes, N. 2020, *PhRvL*, 125, 261104, doi: [10.1103/PhysRevLett.125.261104](https://doi.org/10.1103/PhysRevLett.125.261104)
- Tsaloukidis, L., Koliogiannis, P. S., Kanakis-Pegios, A., & Moustakidis, C. C. 2023, *PhRvD*, 107, 023012, doi: [10.1103/PhysRevD.107.023012](https://doi.org/10.1103/PhysRevD.107.023012)
- Typel, S., & Wolter, H. H. 1999, *NuPhA*, 656, 331, doi: [10.1016/S0375-9474\(99\)00310-3](https://doi.org/10.1016/S0375-9474(99)00310-3)
- Wilms, J., Allen, A., & McCray, R. 2000, *ApJ*, 542, 914, doi: [10.1086/317016](https://doi.org/10.1086/317016)
- Zdunik, J. L., & Haensel, P. 2013, *A&A*, 551, A61, doi: [10.1051/0004-6361/201220697](https://doi.org/10.1051/0004-6361/201220697)